Polymer 325 (2025) 128269

Contents lists available at ScienceDirect

Polymer

journal homepage: www.elsevier.com/locate/polymer

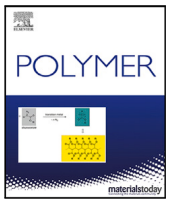

Multiscale molecular simulations of grafted materials

Gianmarco Munaò [a,*], Cosimo Brondi [b,c], Antonio Baldanza [d], Antonio De Nicola [e], Riccardo Chiarcos [f], Michele Laus [f], Michele Perego [g], Giuseppe Scherillo [c], Giuseppe Mensitieri [c], Giuseppe Milano [c,*]

[a] Dipartimento di Scienze Matematiche e Informatiche, Scienze Fisiche e Scienze della Terra, Università degli Studi di Messina, V.le F. Stagno d'Alcontres 31, 98166 Messina, Italy
[b] Dipartimento di Ingegneria e Scienze, Facoltà di Scienze Tecnologiche e dell'Innovazione, Università Mercatorum, 00186 Roma, Italy
[c] Dipartimento di Ingegneria Chimica, dei Materiali e della Produzione Industriale, Università di Napoli "Federico II", Piazzale V. Tecchio 80, 80125 Napoli, Italy
[d] Scuola Superiore Meridionale, 80138 Napoli, Italy
[e] Dipartimento di Calcolo ad Alte Prestazioni, CINECA, 40033, Casalecchio di Reno, Bologna, Italy
[f] Dipartimento di Scienze e Innovazione Tecnologica (DISIT), Università del Piemonte Orientale "A. Avogadro", 15121 Alessandria, Italy
[g] Istituto per la Microelettronica e Microsistemi (IMM), Consiglio Nazionale delle Ricerche (CNR), Via C. Olivetti 2, Agrate Brianza 20864, Italy

ARTICLE INFO

Keywords:
Grafting
Nanoparticles
Polymer melt
Particle-field simulations
Brushes
Potential of mean force

ABSTRACT

An overview of recent applications of hybrid particle-field Molecular Dynamics (hPF-MD) to grafted materials is presented. For such an aim, two classes of materials are considered: polymer nanocomposites and polymer brushes. In the first case, the hybrid approach demonstrates its efficiency to properly relax polymer chains even of high molecular weight. Also, results highlight the role played by configurational entropy of polymer chains in determining the effective (two-body and three-body) nanoparticle–nanoparticle interaction in the melt. A similar role emerges also in the investigation of polymer brushes, where hPF-MD simulations clarify the mechanisms underlying the "grafting to" process, pointing towards a partition by molecular weight of polymer chains. This effect, which causes the segregation of the chains with lower molecular weight in proximity of the substrate surface, is purely entropic and it is originated by the stretching of polymer chains during the grafting to reaction. This picture is also confirmed by a very recent combination of self-consistent field theory with the lattice-based reactive Monte Carlo method which allows to predict for the first time the final composition of the chains grafted on the surfaces.

1. Introduction

In the framework of polymer chemistry, grafting is a procedure in which monomers belonging to a given chain are covalently bonded onto a surface or a substrate [1,2]. For such an aim, one end group of a polymer chain can be appropriately functionalized, allowing the chain to be grafted onto surfaces of different chemical compositions, leading to modifications of chemical–physical properties of the latter. These modifications can include changes in solubility, nano-dimensional morphology and biocompatibility [3,4]. Currently, grafting is largely implemented to modify the properties of both NPs and solid surfaces according to tailored specifications designed for target applications [5,6]. In particular, two well-known applications of grafting to design targeted materials are constituted by grafted nanoparticles (NPs) [7–9] and polymer brushes [10,11]. Both of them represent a transformative class of materials, merging nanoscale precision with tailored surface properties. These hybrid systems have enabled significant advances in applications ranging from biomedical to materials science [12].

Grafted NPs find their most widespread application in the field of polymer nanocomposites. Indeed, it is well known that the macroscopic properties of many polymer melts can be significantly improved by the addition of appropriate fillers, such as inorganic NPs [13–18]. One of the most studied cases is that of silica NPs embedded in a polystyrene (PS) matrix, which has been extensively investigated through both experimental [19–21] and simulation [22–28] approaches. The presence of polymer chains grafted onto the NP surface significantly affects the structure, thermodynamics, and phase behavior of the composite material, as demonstrated in theoretical [29–32], simulation [33–36], and experimental [37,38] studies. In particular, theoretical approaches based on self-consistent field theory [39–42] have successfully shown the effects of the grafting density on solvation free energy, effective interactions and local structure of grafted silica NPs-PS composites.

* Corresponding authors.
E-mail addresses: gmunao@unime.it (G. Munaò), giuseppe.milano@unina.it (G. Milano).

https://doi.org/10.1016/j.polymer.2025.128269
Received 28 December 2024; Received in revised form 4 March 2025; Accepted 10 March 2025
Available online 20 March 2025

The importance of a proper understanding of grafting processes and role played by both grafting density and molecular weight of grafted chains is not limited to nanocomposites materials, but it clearly emerges also in polymer brushes. In this context, an application which is arousing much interest is constituted by block copolymer (BCP)-based nanopatterning methods [43] which allow for the production of a plethora of nanostructures avoiding the limitations typical of conventional photolitographic approaches [44]. Since the orientation of BCP features in thin films, when deposited over a silicon surface, can be successfully controlled through random copolymers (RCP) grafted to the surface of the substrate [45], the microscopic mechanisms underlying the grafting processes become crucial. The generally accepted scenario is that of the "grafting to" reaction from melt, which consists in anchoring an end-functional polymer onto a proper substrate. Although thermodynamic and kinetic aspects of grafting to reactions are currently the object of rather intense investigations [46,47], some relevant aspects still remain uncovered, including the way how the grafting and degrafting reactions are influenced by the molecular weight and polydispersity of polymer chains.

In order to overcome this issue, in the last decades much effort has been devoted to develop suitable simulation and theoretical approaches to study grafted NPs in composite materials and polymer brushes, as comprehensively reported in some recent reviews [48–50]. From these works it emerges that many different computational and theoretical techniques can be applied to investigate both polymer nanocomposites and brushes, including Molecular Dynamics (MD), Brownian Dynamics, Dissipative Particle Dynamics and Monte Carlo (MC) methods [51], as well as PRISM [52], pyPRISM [53], density functional [54] and self-consistent field theories [55]. However, these theoretical approaches, as well as simulation studies based on coarse-grained (CG) models, can be only applied to generic systems and therefore can be hardly implemented for a specific case of interest. On the other hand, all the reviewed simulation approaches based on atomistic representations are computationally very expensive when applied to large systems or to large time-scales. Similar pictures also emerge from Refs. [56,57], where it is clearly stated that atomistic models allow for quantitative comparisons with experiments, but they are also computationally demanding and therefore can be only applied to small systems, with a consequent lack of predictions for grafted long-chain polymers.

Therefore, by focusing our discussion to simulation studies, typically two kinds of approaches are implemented in the literature: those based on generic or CG models on the one hand and those implementing atomistic simulations on the other hand. Both of them show advantages and disadvantages: the former are usually well suited to investigate and understand the basic physical principles of composite materials and polymer brushes, but they lack the chemical detail required for a precise description of these systems. On the other hand, atomistic approaches are very effective in reproducing the local chemical structure of these materials but they are unavoidably restricted to short polymer chain lengths and timescales. In particular, for grafted NPs a proper sampling of polymer chain conformations in the presence of solid NPs is needed. In the case of grafting to reaction, one also needs to understand the outcome of the reactions (which are generally studied through quantum approaches) and include them in a model that takes into account entropic effects due to the chain stretching induced by the presence of the reactive chains in polymer brush.

In order to overcome these limitations through computer simulations, one of the most convenient approaches is to combine traditional MD simulations with a self-consistent field representation of non-bonded interactions [58]. This combination gives rise to the hybrid particle-field Molecular Dynamics (hPF-MD) approach (see Ref. [59] for a recent review). The main purpose of this approach, within the framework provided by the self-consistent field theory, is to obtain the partition function of a single molecule in an external potential $V(\mathbf{r})$, along with a suitable expression of $V(\mathbf{r})$ and its derivatives. According to this formulation, the most computationally expensive part of the MD simulations, which amounts to calculate the non-bonded forces between atoms of different molecules, can be replaced by the evaluation of interactions among each atom and an external potential that depends on the local density at position $\mathbf{r}$. In this framework it is possible to obtain a substantial speed up of the simulation times, allowing for properly relaxing, among others, polymer chains with large molecular weights [60], carbon nanotubes [61,62] and nanocomposite materials [63,64], at the same time maintaining a chemically accurate description of the system.

In the present contribution we report a summary of recently developed hybrid particle-field models when applied for the first time to simulate the formation of nanostructures in grafted NPs and the mechanochemical control leading to selectivity in grafting to reactions. Furthermore, it will be highlighted how the hPF-MD approach allows to successfully model the connection between the chemical detail and the scales needed for a proper representation of grafted materials. Finally, we present a very recent combination of self-consistent field theory with the lattice-based reactive MC method [65] which allows to introduce for the first time the effect of chain stretching on the grafting to reactions and therefore to predict the composition of the chains grafted on the surfaces.

The basics of hPF-MD method are provided in what follows: according to the hybrid representation, the Hamiltonian of a given system in the phase space can be written as [66]:

$$\hat{H}(\Gamma) = \hat{H}_0(\Gamma) + \hat{W}(\Gamma), \tag{1}$$

where $\hat{H}_0$ is the Hamiltonian of a system of molecules with only intramolecular interactions and $\hat{W}(\Gamma)$ keeps into account the non-bonded interactions. Also, Γ indicates a point in the phase space and the symbol $\hat{}$ means that a given variable is a function of the microscopic state represented by Γ. Now, what we need is a proper recipe to calculate $\hat{W}(\Gamma)$. In the self-consistent field theory, we may assume that $\hat{W}(\Gamma)$ depends on Γ only through the particle density $\hat{\phi}(\mathbf{r};\Gamma)$ [66], *i.e.*:

$$\hat{W}(\Gamma) = \hat{W}(\hat{\phi}(\mathbf{r};\Gamma)), \tag{2}$$

which amounts to assume that a single molecule interacts with all other molecules through an external field depending on the density distribution of the latter. This field can be described by an external potential $V_k(\mathbf{r_i})$ which, in turn, can be calculated by performing the functional derivative of the total energy [66]. By assuming for the latter the expression due to Helfand [67]

$$W[\phi_K(\mathbf{r})] = \int d\mathbf{r} \left[\frac{k_B T}{2} \sum_{KK'} \chi_{KK'} \phi_K(\mathbf{r}) \phi_{K'}(\mathbf{r}) + \frac{1}{2} \left(\sum_K \phi_K(\mathbf{r}) - 1 \right)^2 \right], \tag{3}$$

we obtain the following expression for the external potential acting on the ith particle:

$$V_K(\mathbf{r_i}) = k_B T \sum_i \left[\sum_{K'} \chi_{KK'} \phi_K(\mathbf{r_i}) + \frac{1}{k} \left(\sum_K \phi_K(\mathbf{r_i}) - 1 \right) \right]. \tag{4}$$

In Eq. (4) k_B is the Boltzmann constant, T is the temperature, the density field of the species K placed in $\mathbf{r}$ is given by $\phi_K(\mathbf{r})$, k is the isothermal compressibility and $\xi_{KK'}$ are the mean-field interaction parameters between a particle of type K and the density fields of particles of type K'. According to the definition provided by Eq. (4), in the simple case of a binary mixture constituted by two species A and B, the mean field potential of a single particle of type A placed in $\mathbf{r}$ is [66]:

$$V_A(\mathbf{r}) = k_B T [\chi_{AA} \phi_A(\mathbf{r}) + \chi_{AB} \phi_B(\mathbf{r})] + \frac{1}{k} (\phi_A(\mathbf{r}) + \phi_B(\mathbf{r}) - 1), \tag{5}$$

with a similar expression holding for a particle of type B. The force acting on particle A placed in $\mathbf{r}$ can be evaluated by performing the partial derivative of $V_A(\mathbf{r})$ with respect to $\mathbf{r}$. Once known the intramolecular terms and the non-bonded potentials, in close analogy

to the traditional force fields of MD simulations, a hybrid force field representation is obtained for the system at issue. In addition, since one needs to obtain a CG density, the simulation box is usually divided into a certain number of cells n_x, n_y and n_z, along the three coordinate axis. All particles are distributed inside these cells according to their positions in the box, generating a density grid whose resolution depends on the choice of n_x, n_y and n_z. Both density and its derivatives, needed to compute forces and potential energy due to particle-field interactions, can be defined on three-dimensional lattice points obeying the periodic boundary conditions. To evaluate the density function at positions **r** between lattice points it is possible to linearly interpolate values at neighbor lattice points. Also, if in the hPF-MD framework entanglements are not explicitly modeled, polymer chains, due to the softness of potentials, are free to cross each other. This feature is very useful in order to efficiently relax polymer chains with high molecular weight, as will be shown more in detail in the next sections. In addition, it is possible to explicitly restore the entanglements by implementing the slip-string method, as detailed in Ref. [59]. The implementation of the so obtained hPF-MD approach can be done through the specifically developed OCCAM code, whose details can be found in Ref. [68].

The present contribution is structured as follows: in Section 2, we discuss the performances of the hPF-MD approach in studying interfacial properties and potential of mean force for separating grafted silica NPs in a PS melt. In Section 3, we review the capability of the hPF-MD method to shed light on the properties of the brush-thin films interface, and the mechanism through which grafting to reactions can be better controlled and understood. In particular, hPF-MD results emphasize the critical role of the conformational entropy of grafted chains in controlling both the phase behavior of the composite material and the grafting to reactions. In Section 4, we provide a further validation of this picture through a recent approach [65] that combines reactive Grand Canonical MC simulations [69] and Scheutjens–Fleer self-consistent field theory [70]. Finally, conclusions and perspectives are presented in Section 5.

2. Grafted silica nanoparticles in polystyrene melts

2.1. Coarse grained models and relaxation of polymer chains

Even though the hPF-MD method can be successfully applied to atomistic models [63], in what follows we focus our discussion to its application to CG models able to represent both silica grafted NPs and PS chains. A well suited CG representation, introduced in Ref. [71] and validated in Refs. [25,63,72] is presented in Fig. 1. In this model, a PS bead represents a single repeating unit of atactic PS, where the two different beads labeled R and S account for the chirality of the asymmetric carbon atom (Fig. 1A). As far as the silica NP is concerned, each bead groups one SiO_2 unit and is centered on the silicon atom (Fig. 1B). The model for a grafted silica NP is built following the protocol described in Ref. [25], where a variable number of PS chains can be grafted onto the NP surface through a linker unit, constituted by four CG beads. An example showing a silica NP grafted with 4 PS chains is represented in Fig. 1C. To accurately describe the silica NP through the hybrid particle-field representation, it is important to account for the periodic interstitial structure of the NP surface, which may generate an oscillating density field inside the NP core. To overcome this issue, the NP density can be modeled using appropriate spline functions, as successfully implemented in previous hPF-MD studies of silica-PS nanocomposites [63,72,73].

In order to highlight the role played by the both ungrafted (free) and grafted chains in determining the behavior of the composite, it is convenient to describe its structural and thermodynamic properties in terms of grafting density (ρ_g), number of grafted chains (N_g), molecular weight of grafted chains (L_g), number of free chains (N_f) and molecular weight of free chains (L_f). As a first issue, the efficiency of the hPF-MD approach in relaxing polymer chains in the composite materials has to be addressed. For such an aim, a good indication is provided by the computation of the autocorrelation function (ACF) of the end-to-end vector: indeed, the simulation time which is needed to obtain an independent chain configuration (and therefore to loose the memory of the previous one) corresponds to the time that the ACF needs to decay to zero. As shown in Fig. 2A, in the case of a PS melt containing a grafted NP with $\rho_g = 1.0$ chains/nm^2, ACFs of free chains go to zero within less than 13 ns even for high molecular weights, such as $L_f = 2400$. A similar order of magnitude is observed in the case of ungrafted NPs, as seen in the inset. This circumstance testifies both the efficiency of the hPF-MD approach in relaxing PS chains even of high molecular weights and the independence of ACF from the grafting density of the NP. The same efficiency can be deduced also from the analysis of the mean square displacement (MSD), reported in Fig. 2B. Indeed, one can assume that the equilibrium has been reached once each chain moves its center of mass by at least its gyration radius [63]. Finally, the hPF-MD approach can be also successfully used to predict the local arrangement of free and grafted chains, as done in Fig. 2C, where the density profiles of free and grafted chains under different conditions are reported. Interestingly, upon increasing the grafting densities from 0.5 to 1.0 chains/nm^2, the peak of the grafted chains distribution increases, while that of free chains decreases. This behavior amounts to a progressive expulsion of free polymer chains from the grafted corona [74] and it is known as "wet-brush-to-dry-brush" transition, observed also in standard MD simulations of similar systems [22,25]. In this context it is also worth addressing the hPF-MD capability to reproduce interface properties between grafted NPs and PS melt. In particular, in the case of grafted NPs the density fluctuations occur in both all-atom and CG particle–particle models at distances very close to the surface in a range less than one nm, as can be seen, for instance, in Ref. [25]. In the hPF-MD approach the implemented values of the grid spacing are of the same order of magnitude (or smaller) than the distance between the peaks of density profiles obtained by using atomistic and CG simulations with pair potentials. Thus, this interface behavior can be reproduced only on average. On the other hand, as stated in Ref. [63], it is possible to overcome this issue by recovering short-range correlations through very short MD runs, due to their local nature. It is also worth noting that generally these short recovery times are independent on the chain length.

In summary, the hPF-MD approach proves capable of capturing all the essential features of the nanocomposite material. Compared to standard simulation studies that implement particle–particle potentials [22,25], the hPF-MD method offers a significant advantage: it enables the full relaxation of PS chains with high molecular weights. This, in turn, allows for the investigation of equilibrium properties, which are often challenging to address using traditional simulation methods.

As an example, the two-body and three-body potential of mean force (PMF) will be discussed in the following sections.

2.2. Effect of grafting on free energy for nanoparticles separation

In this section we present a protocol, based on the thermodynamic integration, to compute the two-body PMF between a pair of silica NPs. As detailed in many computational studies [75–77] the knowledge of the effective potential is of paramount importance to predict the phase behavior of the composite. For such an aim, the generally adopted procedure is that of preparing a set of many different initial configurations, each one corresponding to two NPs (which, in our case, are embedded inside the PS melt) at a fixed distance from each other, as schematically reported in Fig. 3. Thereafter, one simulation has to be done for each configuration, in which NPs are allowed to rotate but not to translate, in order to guarantee that their mutual distance remains fixed. Once the system reaches the equilibrium, the forces F acting on the centers

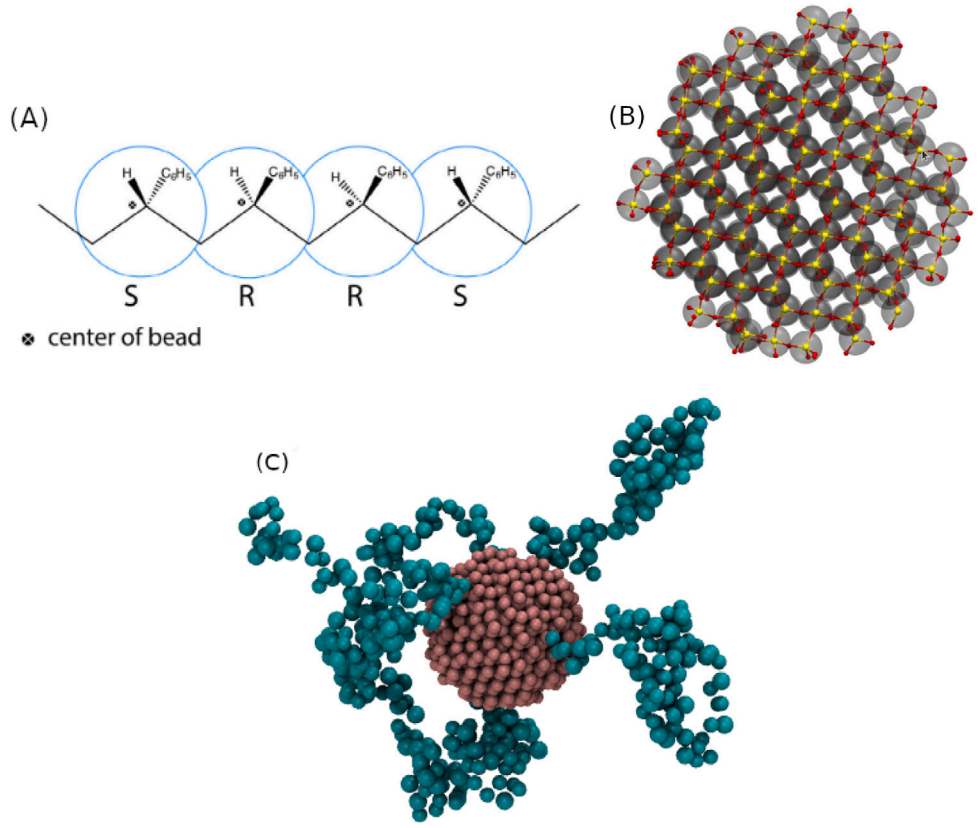

Fig. 1. PS (A), bare (B) and grafted (C) silica NP CG models. In (A) the center of PS beads is indicated by crossed circles and a single bead groups one PS monomer. In (B) the section of silica NP core is shown. Each bead is centered on silicon atoms (in yellow) and corresponds to a SiO_2 unit, while oxygen atoms are given in red. In (C) a snapshot of silica NP (in pink) grafted with 5 PS chains, each one constituted by 84 beads (in cyan), is given. Panels A and B are reproduced from Eur. Phys. J. Spec. Top. 2016 225, 1817. https://doi.org/10.1140/epjst/e2016-60127-0. (For interpretation of the references to color in this figure legend, the reader is referred to the web version of this article.)

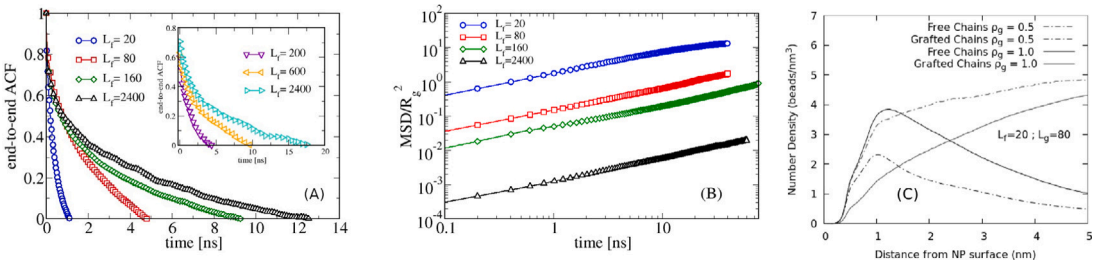

Fig. 2. (A): ACF of the end-to-end vector for free PS chains containing a grafted silica NP with $\rho_g = 1.0$ chains/nm^2 and $L_g = 80$. Inset: same for a PS melt with a ungrafted silica NP (see Ref. [63]). Values of L_f are in the legends. (B): MSD of the center of mass of free chains normalized by the gyration radius (R_g) as a function of the time in a logarithmic scale for $\rho_g = 1.0$ chains/nm^2, $L_g = 80$ and various L_f. Values of R_g are 0.92, 1.99, 2.83 and 8.42 nm for $L_f = 20$, 80, 160 and 2400, respectively. (C): bead number density of free and grafted chains for $\rho_g = 0.5$ (dashed lines) and 1.0 (full lines) chains/nm^2 as a function of the distance from the NP surface. Panel (C) is reproduced from Nanoscale 2018, 10, 21,656–21,670. https://doi.org/10.1039/C8NR05135F.

of mass of the two NPs can be calculated, averaged and integrated over the interparticle distances r according to the equation:

$$U(r) = -\int_{r_{\min}}^{r_{\max}} \bar{F}(r)dr\,, \tag{6}$$

where $U(r)$ is the PMF, $r_{\min}$ is the NP diameter and $r_{\max}$ is the interparticle distance where the potential can be confidently assumed equal to zero. Also, it is worth noting that $U(r)$ is only one of the two contributions that must be taken into account to calculate the total interaction between a pair of NPs; indeed, one also needs to compute the direct interaction between the NP cores, usually modeled through the Hamaker potential [78]. A proper parameterization of this potential can be done on the basis of atomistic simulations, following the prescription reported in Ref. [79].

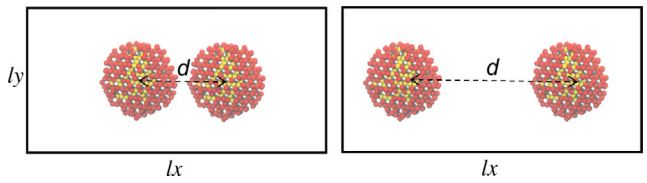

Fig. 3. Schematic representation of the protocol for calculating the two-body PMF upon increasing the distance between a pair of NPs.
Source: The Figure is reproduced from Nanoscale 2018, 10, 21,656–21,670. https://doi.org/10.1039/C8NR05135F.

The knowledge of effective NP–NP interactions may allow, in principle, to know the phase behavior of the composite material, which

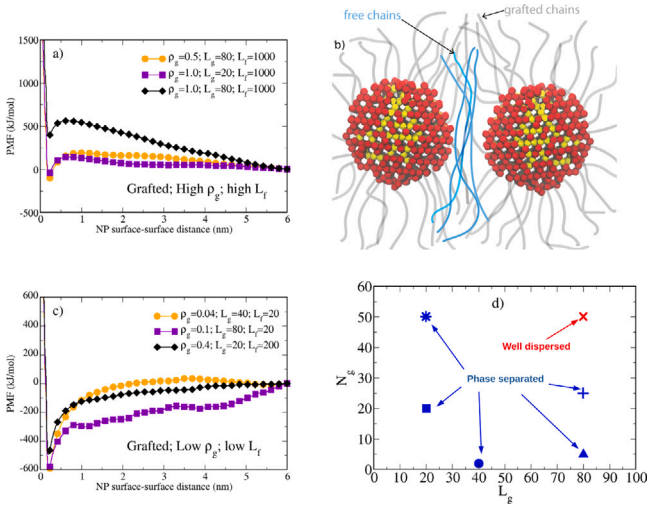

Fig. 4. Comparison among two-body PMF of grafted NPs for high (a) and low (c) grafted densities and molecular weight of free chains. The confinement of PS chains between two grafted NPs is pictorially represented in panel (b), where grafted and free chains are reproduced in gray and blue colors, respectively. A schematic phase diagram is reported in panel (d). (For interpretation of the references to color in this figure legend, the reader is referred to the web version of this article.)
Source: All panels of the Figure are reproduced from Nanoscale 2018, 10, 21,656–21,670. https://doi.org/10.1039/C8NR05135F.

is a crucial issue in order to predict the composite final properties. A systematic study of PMF as a function of grafting density and polymer molecular weight is therefore very helpful to identify the different regimes that can be expected. In particular, the role played by the grafting density needs to be properly taken into account and, for such an aim, a wide range of regimes, going from 0.04 to 1 chains/nm^2 has been considered. A summarizing comparison among the two-body PMF between a pair of grafted NPs is shown in Fig. 4, along a cartoon showing the configurations of free and grafted chains confined between the NPs. As shown in panel (a), the two-body PMF is significantly repulsive for high values of both ρ_g, L_g and L_f. Upon lowering ρ_g or L_g, the PMF shows a slightly negative minimum before going to zero even for low interparticle distances. The NP–NP repulsion observed for high values of ρ_g or L_g can be ascribed to the entropy loss (and therefore free energy increase) due to both the stretching of grafted chains and the steric repulsion among them, as sketched in the cartoon of panel (b). Conversely, for low grafting densities the two-body PMF is attractive regardless the specific values of L_g and L_f, as shown in panel (c). It may be worth noting that this behavior is different from that reported in Ref. [39], where the PMF between a pair of grafted silica-PS plates is calculated through the self-consistent field theory. Indeed, in that case it was found that upon decreasing the molecular weight of free chains, a progressively more repulsive PMF between the plates is obtained. The opposite behavior is found when free chains are of much larger molecular weight of grafted chains. These results suggest a role played by the curvature of the grafted surface: for high curvature (as in the case of NPs) the molecular weight of free chains plays only a marginal role, which becomes significant when the curvature vanishes, as in the case of plates.

On the basis of the behavior documented in Fig. 4, upon considering a collection of several NPs in a PS melt, one should obtain a dispersed phase when the two-body PMF is significantly repulsive and a separation of all NPs from the melt when it becomes attractive. This can be verified by calculating the second virial coefficient as detailed in Ref. [72]: indeed, it is known that values of $B_2 < 0$ ($B_2 > 0$) indicate that attractive (repulsive) interactions prevail [80], therefore providing indications on the overall phase behavior of the composite. The resulting phase diagram, for some selected values of ρ_g and L_g, is shown in Fig. 4d.

On the other hand, from the knowledge of experimental phase diagrams of silica-PS nanocomposites [7,16] it emerges that well dispersed conditions and phase separations are not the only phases that can be found in these systems. Indeed, complex structures including strings, connected sheets and small clusters are also observed, their appearance depending on specific values of grafting densities and molecular weight of free and grafted chains. However, since the existence of such structures is usually due to a competition between attractive and repulsive interactions [81,82], their appearance cannot be justified on the basis of the two-body PMF described so far. This apparent mismatch can be justified on the basis of two implicit assumptions that have been done so far:

- Multibody contributions to the effective interactions have been neglected.
- A monodisperse distribution of molecular weights of polymer chains has been assumed.

In particular, with reference to the first point, in both experimental [16] and theoretical [83] studies on polymer nanocomposites it has been underlined that in dense systems multi-particle contributions to the PMF cannot be neglected. In addition, a huge number of experimental [84–88] and simulation studies [30,31,89,90] have shown that the existence of a polydispersity on chains distribution can significantly affect static and dynamic properties of the composite material.

This circumstance calls for the explicit inclusion of three-body interactions and polymer dispersity in the calculation of the PMF, as shall be detailed in the next section.

2.3. Role of multibody effects and polymer bidispersity on patterns formation

A pictorial representation of the protocol suited for the calculation of three-body PMF is given in Fig. 5: in this case, beside the two NPs taken into account when computing two-body PMF, also a third NP is needed, that must be placed perpendicularly to the vector joining the centers of mass of the first two NPs. Similarly to the protocol adopted for the computation of the two-body interaction, also in this case the distance d between the first two NPs must be progressively increased, by keeping fixed the position of the third NP. Then, the forces and the effective potentials can be computed according to the previous procedure. The presence of the third NP makes the three-body contribution to the total PMF maximum when it is as close as possible to the other two NPs. In addition, it is also possible to increase the distance D between the third NP and the midpoint of the line joining the first two NPs, in order to obtain an estimate of the short- or long-range nature of the three-body contribution.

As for the role played by the polymer dispersity, by limiting ourself to the case of a bimodal distribution of molecular weights, it is possible to introduce the bidispersity index (BDI), defined as [73]:

$$BDI = M_w/M_n\,, \tag{7}$$

where M_w and M_n are the weight average molecular weight and the number average molecular weight, respectively, defined as:

$$M_w = \frac{\sum_i N_i M_i^2}{\sum_i N_i M_i}; \qquad M_n = \frac{\sum_i N_i M_i}{\sum_i N_i}\,, \tag{8}$$

where N_i and M_i indicate the number of chains with a given molecular weight and the number of beads belonging to each of these chains. Accordingly, the bidispersity indexes of free and grafted chains shall be indicated as BDI_f and BDI_g, respectively.

The role played by both three-body effects and bidispersity of polymer chains on the effective NP–NP interaction is summarized in Fig. 6. It emerges that for intermediate/high grafting densities (*i.e.* $\rho_g = 0.5$ and $\rho_g = 1.0$ chains/nm^2) the addition of the third NP

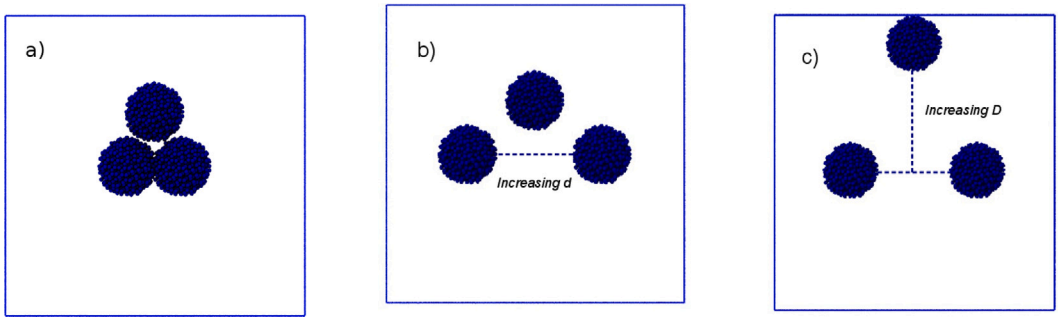

Fig. 5. Schematic procedure for the calculation of the three-body PMF: starting from a configuration where all NPs are in close contact (a), the distance d between the first two NPs increases, leaving unchanged the position of the third NP (b). The short or long-range nature of the three-body PMF can be determined by increasing the distance D between the third NP and the center of the line joining the centers of mass of the first two NPs (c).
Source: The Figure is reproduced from Macromolecules 2019, 52, 8826–8839. https://doi.org/10.1021/acs.macromol.9b01367.

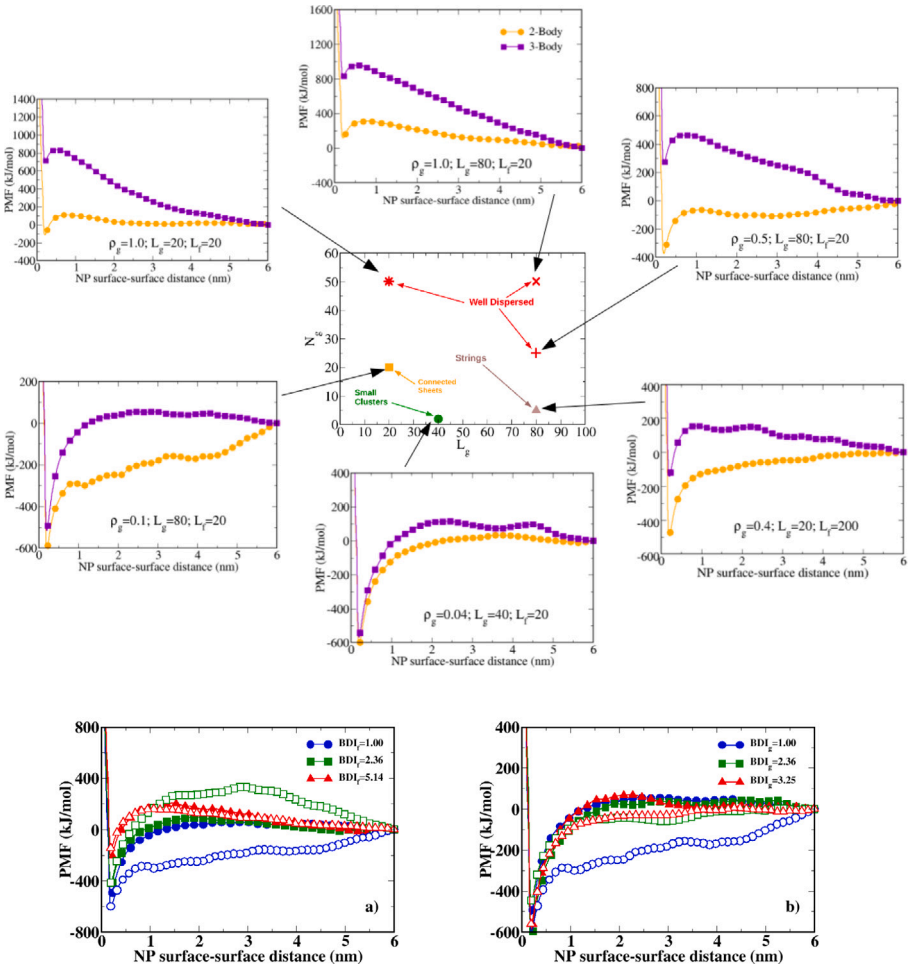

Fig. 6. Top: schematic morphology diagram for grafted NPs embedded in a PS matrix, drawn by considering the three-body PMF and calculating the second virial coefficient. Different colors are used for well dispersed, strings, connected sheets and small clusters regions. The behaviors of two-body and three-body PMF are also reported for enhancing their relation to the morphology diagram. Bottom: comparison between two-body (open symbols) and three-body (full symbols) PMF between grafted NPs with $\rho_g = 0.1$ chains/nm^2 upon increasing BDI_f (a) and BDI_g (b). Top panels are reproduced from Nanoscale 2018, 10, 21,656–21,670. https://doi.org/10.1039/C8NR05135F.

strengthens the repulsive behavior of the PMF. As already observed for the two-body case, this is mainly due to the entropy loss (with the corresponding free energy increase) due to the stretching of grafted chains and increase of the steric repulsion among them, progressively more enhanced as close as the NPs are [72,83]. More interesting behaviors are observed for low grafting densities: indeed, under these conditions all three-body PMFs show the existence of a short-range attraction followed by a longer-range repulsion, compatibly with the onset of aggregated structures, as theoretically predicted [91,92]. In particular, the observed PMFs are compatible with the onset of clusters, planar structures and strings, which have been experimentally observed [7,16]. Interestingly, these findings qualitatively agree also with results based on dissipative particle dynamics (DPD) simulations of Lu and co-workers [90], in which has been shown that anisotropic self-assembled structures can be achieved only by setting moderate grafted chain lengths and grafting densities. As a further interesting datum, upon grafting NPs with low-molecular-weight chains, the NP

aggregation was always found; however, this circumstance has not been investigated in the hPF-MD approach.

The effect of bidispersity is presented in the bottom panels of Fig. 6, where, for a grafted NP with $\rho_g = 0.1$ chains/nm^2 the increase of BDI_f (a) and BDI_g has been separately considered. In the first case, the comparison with the two-body PMF shows that in the monodisperse condition the three-body PMF is more repulsive than the two-body counterpart, while for $BDI_f = 2.36$ this trend is reversed and for $BDI_f = 5.14$ two- and three-body PMF similarly behave. This suggests that in this case multibody effects and the wettability of the NP surface, influenced by the increase of BDI_f are non-trivially combined, generating a complex, non-monotonic dependence of the resulting PMF on the bidispersity. On the other hand, the effect of increasing BDI_g (b) is more clear: indeed, in all cases the repulsion increases when going from two- to three-body interactions, as also expected on the basis of experimental studies of bimodal NPs [86]. Noteworthy, also in this case a qualitative agreement is found with results reported in Ref. [90], where it was stated that when bimodal grafted NPs are considered, an entropy gain for the polymer matrix penetration inside the brush is observed, promoting a well-dispersed condition.

Summarizing, what finally emerges from the combined analysis of structure, free energy and multibody effects of grafted silica NPs in PS melt is that a leading role is played by the conformational entropy of polymer chains. Indeed, it is worth pointing out that all these effects are purely entropic, since no energetic contribution among polymer chains (which are all of the same chemical species) has to be addressed. Therefore, the gain or loose of chain entropy is enough to promote or hinder a given phase behavior and to provide the final properties of the composite.

3. Silicon surfaces grafted with poly(styrene-r-methyl methacrylate) random copolymers

3.1. Interface between polymer brushes and thin films

As anticipated in the Introduction, the second class of grafted materials reviewed in the present contribution concerns polymer brushes. In particular, it has been pointed out [45] the importance of a proper dealing of the interface between BCP thin films and solid substrates grafted with RCP brushes. When studying the spin-coating of a BCP solution on a silicon substrate with RCP grafted onto its surface, it is worth noting that the infiltration of the solvent in the BCP film may increase the chain mobility, reducing the free-energy barriers of the process [93]. In these cases, a proper characterization of the RCP/BPC interface could, in principle, depends on a number of factors:

- The molecular weight and grafting density of the brush.
- The thickness of the BCP film.
- The amount of the residual solvent.

It is worth pointing out that when simulating polymer brushes the grafting density regime is always less or at most equal to the mushroom regime [74], according to the experimental values of the grafting density achieved during the grafting to reactions. To clarify the effects of these parameters on the brush/thin film interface, the hPF-MD approach can be applied to poly(styrene)-b-poly(methyl methacrylate) (PS-b-PMMA) BCP thin films spin-coated on a functional hydroxyl-terminated poly(styrene-r-methyl methacrylate) [P(S-r-MMA)] RCP brush layer grafted onto a silica substrate [93]. Deuterated toluene can be employed as the solvent, providing a suitable medium for the simulation and experimental comparison.

To perform such simulations, CG models of copolymers, substrate, and solvent must be developed. Following the mapping proposed in Ref. [93], the silica substrate is modeled as a collection of 18,720 beads arranged in a hexagonal configuration, forming eight connected layers with a total thickness of 4.9 nm. This representation ensures a realistic description of the substrate geometry and surface properties.

The RCP and BCP chains are represented as sequences—random for RCP and ordered for BCP—of two types of beads. Each bead corresponds to five PMMA or six PS units. The mapping scheme for an RCP chain is shown in the left panel of Fig. 7, where the random arrangement of PMMA and PS beads reflects the copolymer's structure.

The solvent is modeled as a single bead representing five toluene molecules. Additionally, to accurately simulate the BCP–air interface, vacuum beads must be explicitly included, as proposed in Ref. [94]. This ensures a proper description of the interfacial effects and phase separation phenomena occurring at the thin film boundary. The resulting CG system is depicted in the right panel of Fig. 7, which integrates substrate, brush layer, copolymer thin film, solvent, and vacuum components into a unified framework.

To reduce the number of simulation parameters, a fixed grafting density is considered in this case study. This choice allows for a focused investigation of the interfacial properties and the role of conformational entropy in determining the behavior of the brush/thin film system.

The role played by the solvent at the RCP/BCP interface can be investigated by calculating density profiles as a function of the toluene concentration and the thickness of the BCP film. Such density profiles, calculated along the axis orthogonal to the interface, are reported in Fig. 8 for a brush molecular weight of 19.5 kg·mol^{-1}: interestingly, while for a BCP thickness of 30 nm (left) no significant effects of the toluene concentration are found, for BCP=75 nm one clearly observes that the amount of BCP at the interface decreases upon increasing the solvent concentration. In addition, also the density profiles of the grafted substrate change, but from the simple visual inspection of the figure, one cannot quantify this change. In this context, a rule to compute how the RCP/BCP interface depends on both solvent concentration, BCP thickness and RCP molecular weight can be very helpful. For such an aim, according to the prescription reported in Ref. [95], it is possible to define an interpenetration length (which provides an indication of the thickness of the interface) as:

$$\xi = \int dz \cdot \rho_1(z) \cdot \rho_2(z), \tag{9}$$

where $\rho_1(z)$ and $\rho_2(z)$ are the density profiles of RCP brush and BCP film, respectively, normalized by their bulk values. A pictorial representation of the interpenetration region is given in the left panel of Fig. 9, while values of ξ, calculated according to Eq. (9), are collectively reported in the right panel of Fig. 9. It emerges that ξ decreases upon increasing the toluene concentration and increases with the molecular weight of RCP. Conversely, the thickness of the BCP film has a little effect on the interpenetration length and, therefore, on the RCP/BCP interface. Interestingly, it emerges that, apart the role played by the solvent, it is the molecular weight of the brush layer which plays the more significant role in characterizing the interface with the thin film. Therefore, a proper control of brush properties and the mechanisms underlying such properties becomes of paramount importance to investigate this kind of interfaces, as will be further demonstrated in the next section.

3.2. Mechanochemical control in grafting to reactions

In order to shed light on the mechanisms responsible of the grafting to reactions, and on the role played by configurational entropy of polymer chains in this context, it is possible to separately simulate through the hPF-MD approach the different steps of the grafting to process. In particular, it is possible to first model the pre-reaction step by simulating the silica substrate, initially grafted by deuterated random copolymer chains, in contact with fully hydrogenated random copolymer chains, as done in Ref. [96]. Then, one may assume that a single hydrogenated copolymer chain becomes grafted onto the substrate (reaction step), and, consequently, that a single deuterated chain detaches from the substrate surface (post-reaction step). The above said process is schematically reported in Fig. 10.

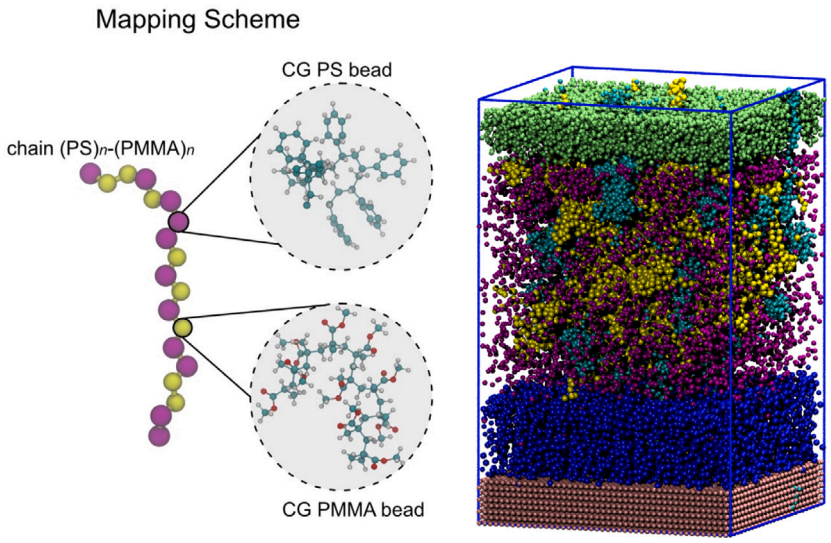

Fig. 7. Left: CG representation of a [P(S-r-MMA)] RCP chain. A single bead groups five PMMA (yellow beads) or six PS (purple beads) repeating units. Right: typical example of CG system suited to be studied through hPF-MD approach. Silica substrate is depicted in pink, RCP chains in blue, BCP chains in yellow and purple, toluene in cyan and vacuum particles in green. (For interpretation of the references to color in this figure legend, the reader is referred to the web version of this article.)

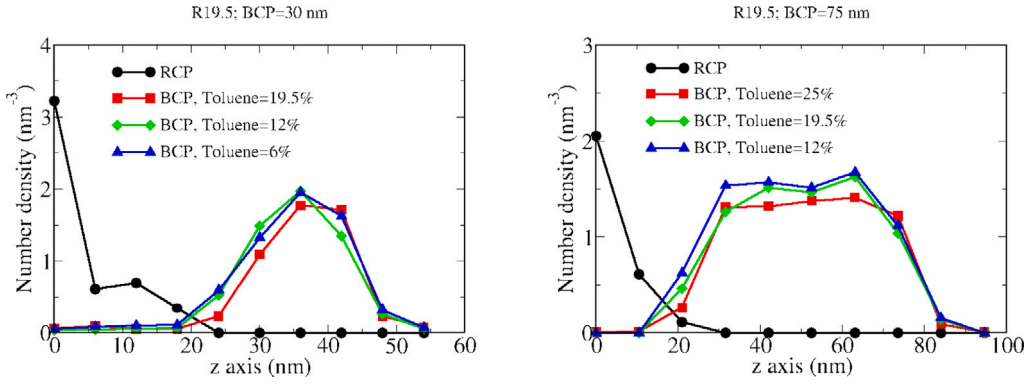

Fig. 8. Density profiles of BCP and grafted substrate for systems with a brush molecular weight of 19.5 kg·mol^{-1} and two different BCP film thicknesses, namely 30 nm (left) and 75 nm (right). Density profiles are shown as a function of the solvent concentration.

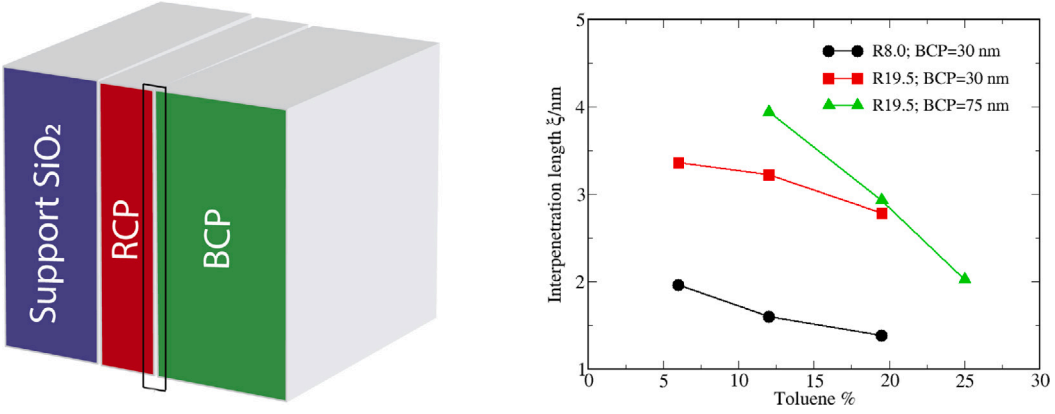

Fig. 9. Left: pictorial representation of the interpenetration region (black empty rectangle) between BCP film (in green) and RCP brush (in red). The silica substrate is also represented (in blue). Right: values of the interpenetration length ξ as a function of the toluene concentration for different values of RCP molecular weights and BCP film thicknesses. (For interpretation of the references to color in this figure legend, the reader is referred to the web version of this article.)

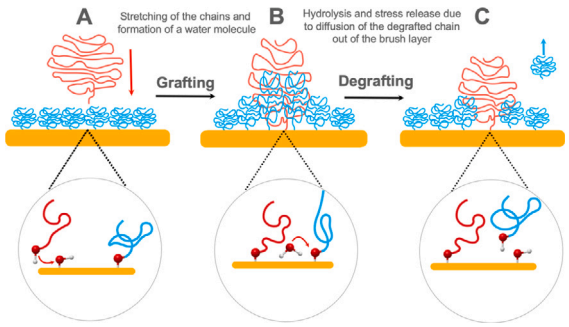

Fig. 10. Schematic representation of the mechanochemically driven grafting to mechanism.
Source: The Figure is reproduced from Macromolecules 2021, 54, 499–508. https://pubs.acs.org/doi/10.1021/acs.macromol.0c02142.

In the course of the whole process, it is worth to investigate the role played by the chain stretching in determining the detachment of deuterated chains. For such an aim, still following what have been done in Ref. [96], it is convenient to consider two cases of high (R38.6) and low (R1.7) molecular weights of the hydrogenated chain, corresponding to 38,600 and 1700 g·mol^{-1}, respectively, while setting the molecular weight of the (monodisperse) deuterated chains to the intermediate value of 19,500 g·mol^{-1} (Rd19.5). In this way, it is possible to clearly identify the entropic effect due to the chain stretching, which, in turns, depends on the molecular weight of the chains. This effect can be investigated by computing the distributions of end-to-end distances of Rd19.5 chains which are placed far from or adjacent to the incoming R1.7 or R38.6 chain, during the reaction step. All chains in the brush layer far away from the incoming one can be considered unperturbed. The resulting probability distributions of the end-to-end distances are reported in Fig. 11 for the different cases where a R38.6 chain becomes grafted to the substrate (a) and after the degrafting (b) of an adjacent chain. The same distributions are computed for an incoming R1.7 chain (c and d). It is clearly observed that once a R38.6 chain becomes grafted to the brush layer, the distribution of adjacent chains takes significantly higher values than that of the unperturbed chains (Fig. 11a): this finding points to a remarkable stretching of the adjacent chains. On the other hand, when one of these stretched chains degrafts from the substrate, the distributions of adjacent and unperturbed chains become very similar (Fig. 11b). In the case where the incoming chains has a significant lower molecular weight (R1.7), the distribution of end-to-end distances of the adjacent chains shows only a slight stretching (Fig. 11c). Once again, the distribution of unperturbed chains is practically restored upon degrafting one of the adjacent chains (Fig. 11d).

According to the picture emerging from this analysis, the reactivity of the systems depends on the degree of stretching (and therefore on the conformational entropy) of the brush layer due to the entering of additional polymer chains. Therefore, there is a "*mechanochemical control*" at work which underlies the whole grafting to process. In this framework, a further consideration immediately arises: the mechanism described so far should imply a preference of chains with low molecular weight to graft the substrate, in comparison to chains with high molecular weight. Therefore, one should be able to verify that, by preparing a blend with different molecular weights (therefore, in the pre-reaction step), the low-molecular weight component should preferentially react with the silicon surface [97]. This can be verified by investigating the behavior of an equimolar polymer blend of partly deuterated hydroxy terminated poly(styrene d_8-st-methyl methacrylate) copolymer with average molecular weight of 11,200 g·mol^{-1} (R11.2) and a hydroxy terminated poly(styrene-st-methyl methacrylate) copolymer with molecular weight of 5400 g·mol^{-1} (R5.4), as done in Ref. [97]. The main results of this investigation are presented in Fig. 12, in which the distribution of the number of contact (a) and of the time fraction (b)

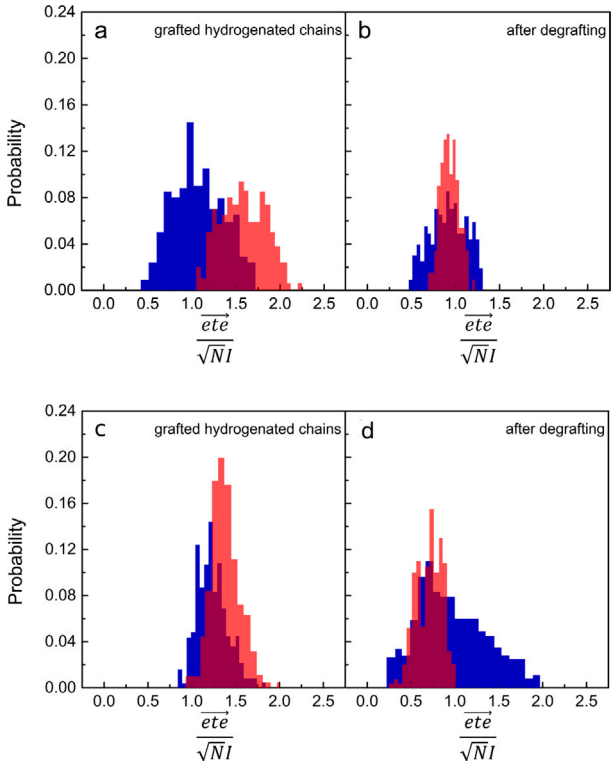

Fig. 11. Probability distribution of the end-to-end distances (normalized by the ideal value) for unperturbed (blue) and adjacent (red) grafted chains: a, R38.6, reaction step; b, R38.6, post-reaction step; c, R1.7, reaction step; d, R1.7, post-reaction step. (For interpretation of the references to color in this figure legend, the reader is referred to the web version of this article.)
Source: The Figure is reproduced from Macromolecules 2021, 54, 499–508. https://pubs.acs.org/doi/10.1021/acs.macromol.0c02142.

spent by chain ends on the surface is reported. As visible, the number of chain ends of R5.4 in contacts with the silica surface is significantly higher than that of R11.2: indeed, the calculation of the average values of contacts $\langle N \rangle$ provides $\langle N \rangle \approx 6$ for R5.4 and $\langle N \rangle \approx 1.8$ for R11.2. In addition, it also emerges that the chain ends belonging to R5.4 spend more time on the silica surface than those belonging to R11.2.

Further indications on the way how chains of different molecular weight arrange themselves onto the silica substrate can be obtained by computing the surface covered by chains. This can be done, in turn, by calculating the components of the gyration radius, as described in Ref. [97]. As a result, it emerges that the surface covered by a single R5.4 chain ($\approx$ 6 nm^2) is much lower that covered by a single R11.2 chain ($\approx$ 15 nm^2). However, the sum over all chains provides a value of $\approx$ 35 nm^2 for R5.4 chains and $\approx$ 25 nm^2 for R11.2 chains, therefore confirming the propensity of chains with the lower molecular weight to graft the silica substrate. Two typical configurations of the system, showing the different arrangements of the chains close to the surface are shown in Fig. 13.

An immediate consequence of this scenario is the occurrence of a molecular weight partitioning during the grafting to reaction, where the lower molecular weight component is selectively incorporated into the brush layer [97]. This selectivity arises from the segregation of shorter chains near the substrate/polymer interface prior to the grafting process [98]. It is important to emphasize that the origin of this selectivity is purely entropic. Specifically, it stems from the differences in the conformational entropy of polymer chains, which ultimately dictates the conditions and outcome of the grafting to reactions.

4. Reactive Grand Canonical Monte Carlo simulations

We conclude our overview of molecular models suited to investigate grafted materials by discussing a hybrid approach [65] that

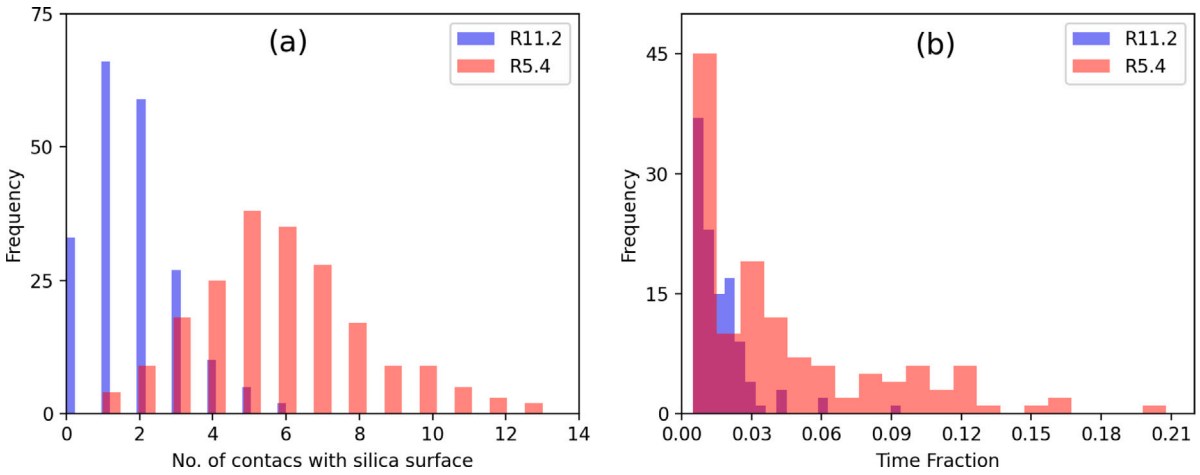

Fig. 12. Distribution of: (a) number of contacts of a chain end with the silica surface; (b) time fraction spent by chain ends on the surface.

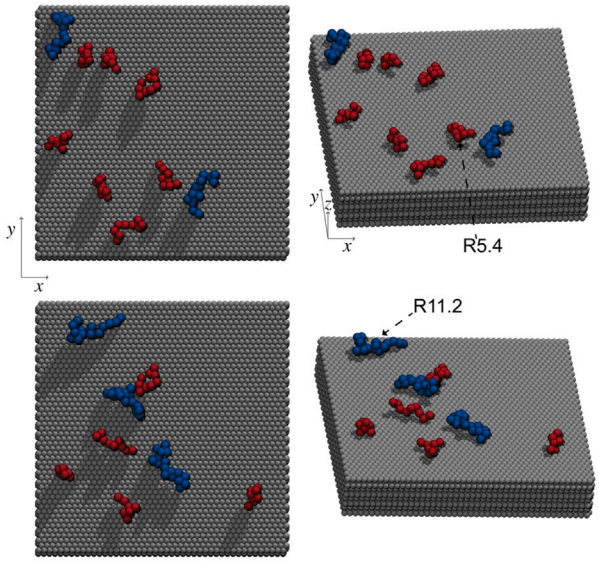

Fig. 13. Representative configurations of adsorbed R5.4 (in red) and R11.2 (in blue) polymer chains. The layers of silica supports are reported in gray. For both configurations the total percentage of surface coverage is ≈ 7%. Other polymer chains are omitted for clarity. (For interpretation of the references to color in this figure legend, the reader is referred to the web version of this article.)

combines reactive Grand Canonical MC (rGCMC) simulations [69] and Scheutjens–Fleer self-consistent field (SF-SCF) [70] theory. This approach has been developed to theoretically elucidate the mechanisms that regulate the competing grafting to process that occurs between low-molecular weight (short) and high-molecular weight (long) chains. By means of this procedure, it is possible to combine the benefits of both the rGCMC (accurate sampling of equilibrium properties of the system under scrutiny) and the SF-SCF (sampling performed at a less expensive computational cost by reducing a many-chain problem to a one-chain problem) approaches. In the specific case of mixtures of hydroxy-terminated poly(styrene-st-methyl methacrylate) (hydrogenated species, h-PS-PMMA) and partly deuterated hydroxy-terminated poly(styrene d8-st-methyl methacrylate) (deuterated species, d-PS-PMMA) [97,98], grafting densities can be predicted by rGCMC and then used to predict the density profiles through the SC-SCF method.

According to the protocol implemented in Ref. [65], the model can be developed on a quadratic lattice in a two-steps process:

- The rGCMC is formulated on a bidimensional lattice with periodic boundary conditions adopted in both the lattice directions. The interaction between the silicon (grafting) substrate and the interacting monomer of a single polymeric chain is described as a point that occupies only one lattice site. The interaction with the grafted polymeric chains is accounted only by the nearest neighbor sites *via* an *ad hoc* potential, which is related to the loss of conformational entropy of the macromolecules in the brush [65]. In this way, the grafted phase is equilibrated with an external reservoir (bulk phase) by exchanging and moving the macromolecules through GCMC trials that are accepted or rejected according to the Metropolis acceptance criterion [99].
- The SC-SCF is formulated in such a way that the structural architecture of the molecule can be built along the third direction of the lattice model (perpendicular to the substrate surface) and the conformational stiffness of the grafted macromolecules can be accounted by implementing the second-order Markov approximation [100].

Full prediction of the grafting density Σ can be performed by rGCMC on blends at different molecular weights MW_h and different compositions $\phi_{h,bulk}$ of the hydrogenated species without any use of parameters retrieved from experiments on blends, as shown in panels (a) and (b) of Fig. 14. When investigating the effects of MW_h (Fig. 14a), results reveal a decreasing trend for h-PS-PMMA, while an increasing trend for d-PS-PMMA is noticed. The observed behavior suggests that the hydrogenated chains are affected by a minor degree of reaction with the silicon substrate when MW_h increases, in favor of an improved affinity for deuterated chains. These findings point out the preferential grafting of shorter chains at expenses of longer ones, regardless the chemical nature of the polymer chain. Upon investigating the effects of blend composition (Fig. 14b), it is observed an opposite trend: the grafting density of hydrogenated species increases with the molar fraction, while the one of deuterated species decreases. Also in this case, this finding can be ascribed to an higher propensity of the lower molecular weight compounds to react with the silicon substrate, the more being the molar fraction of d-PS-PMMA in bulk the more being the brush region enriched of this shorter polymer chain.

Grafting densities predicted by the model and validated by experiments can be therefore implemented to predict morphological features of the obtained brushes, also in this case on blends at different MW_h and $\phi_{h,bulk}$ (panels (c) and (d) of Fig. 14). In cases where MW_h increases (Fig. 14c), the increasing trend of the brush average thickness H suggests that long chains induce not only a wider distribution of the interphase region, but also an increase in the average value of the brush height. In this way it is unveiled that the average trend of H can be attributed to hydrogenated chains that become progressively longer

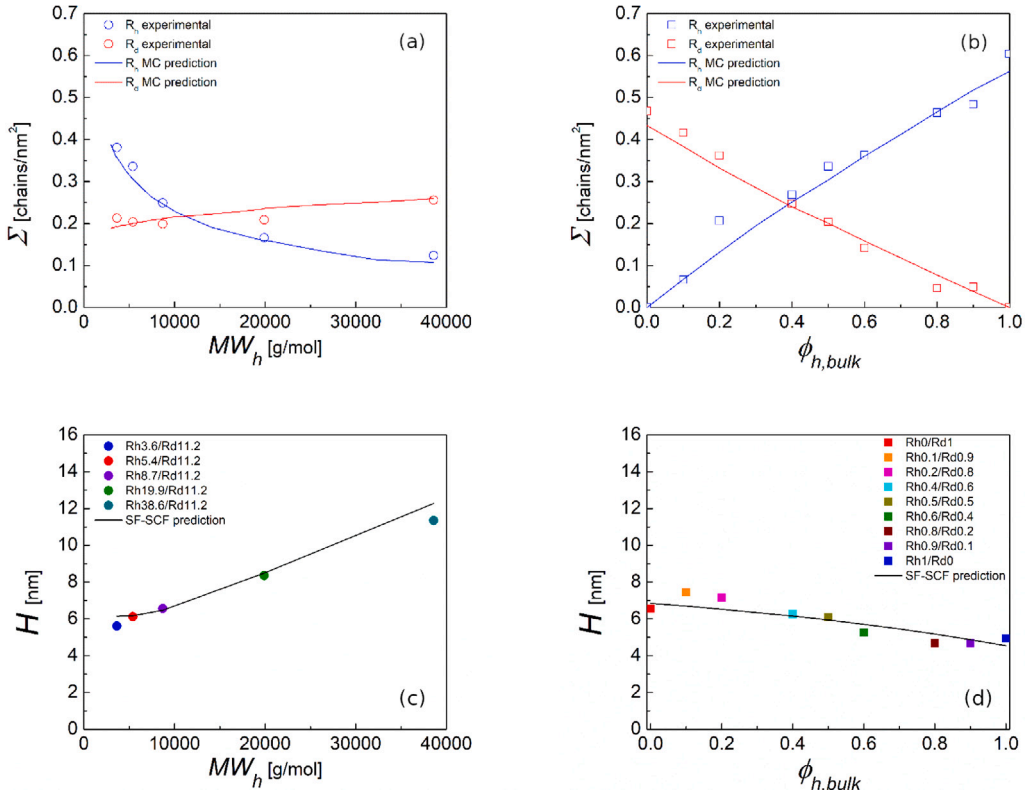

Fig. 14. Grafting density Σ as function of the hydrogenated molecular weight MW_h (a) and of the hydrogenated molar fraction within the bulk $\phi_{h,bulk}$ (b) for binary samples: comparison between the experimental data from Refs. [97,98] and the MC prediction. Brush height H as function of MW_h (c) and of $\phi_{h,bulk}$ (d) for binary samples: comparison between the experimental data from Refs. [97,98] and the SF-SCF prediction.
Source: All panels are reproduced from Polymer 2024, 294, 126737. https://www.sciencedirect.com/science/article/pii/S0032386124000727?via%3Dihub.

and thus reach higher distances, while the deuterated species only change their distribution and always occupy the same portion of the brush region. When dealing with results related to the effects of blend composition (Fig. 14d), it can be observed that H tends to decrease with $\phi_{h,bulk}$, suggesting that a lower concentration of the longer chains (being in this case the deuterated species) within the bulk leads to shorter density profiles within the interphase region.

The model outcomes, parametrized and validated through experimental results, demonstrate the successful viability of novel hybrid technique. Moreover, by combining rGCMC and SF-SCF methods, it is also possible to simulate brush properties, which are hardly measured by experiments such as the local thickness and the surface roughness of the experimental samples [65]. More in general, the proposed approach may represent a fast and accurate tool used to identify optimal parameters useful to realize engineered surfaces obtained by grafting to reactions.

5. Summary and perspectives

In this study, we reviewed two recent applications of the hPF-MD approach to grafted materials. Specifically, we examined grafted silica NPs in PS melts and silica substrates grafted with random copolymer chains. The hPF-MD method has demonstrated exceptional effectiveness in relaxing polymer chains, even those with high molecular weights.

Our findings underscore the critical role of conformational entropy in polymer chains, which significantly influences effective NP–NP interactions and the resulting phase behavior of composite materials. In particular, the hPF-MD approach allows the direct evaluation of the potential of mean force even between NPs grafted by polymer chains with high molecular weight, an issue unaffordable by standard approaches based on pair-potential simulations.

Moreover, hPF-MD simulations provided valuable insights into the microscopic mechanisms underlying the grafting to process in random copolymer-grafted silica substrates. In these systems, conformational entropy was again shown to play a pivotal role, as the final grafting density of the polymer brush strongly depends on chain stretching during the grafting process. Also, the hybrid approach allows a direct comparison with experimental data, along with the possibility to efficiently simulate large systems, in which substrate, brush, solvent and thin film can be properly taken into account.

By synthesizing results from both systems, we highlight the ability of the hPF-MD technique to develop molecular models that elucidate phenomena on scales inaccessible to conventional approaches. These phenomena include the morphology of NP aggregates, the behavior of block and random copolymers in solvent environments, and the ubiquitous entropy loss associated with chain stretching.

Further advances are achieved by combining reactive Grand Canonical Monte Carlo (rGCMC) with the Scheutjens–Fleer self-consistent Field method. This combined approach enables accurate predictions of final grafting densities in polymer brushes, representing a significant improvement over the current state of the art. Also, the implementation of MC-based approaches may allow to improve sampling also in molecular models containing NPs, due to the capability of this method to efficiently sample displacement and rotation of NPs, with a subsequent reduction of simulation times.

The methodologies reviewed here open several directions for future research on grafted materials. Particularly interesting is the clarification of kinetic effects and their interplay with thermodynamic factors during grafting to processes. Understanding these interactions is crucial for achieving precise control over grafted materials. To this end, extending both hPF-MD and rGCMC approaches, as well as their integration, to kinetic schemes could provide powerful simulation tools for gaining molecular-level insights.

CRediT authorship contribution statement

Gianmarco Munaò: Writing – original draft, Conceptualization. **Cosimo Brondi:** Writing – review & editing. **Antonio Baldanza:** Writing – review & editing. **Antonio De Nicola:** Writing – review & editing. **Riccardo Chiarcos:** Writing – review & editing. **Michele Laus:** Writing – review & editing. **Michele Perego:** Writing – review & editing. **Giuseppe Scherillo:** Writing – review & editing. **Giuseppe Mensitieri:** Writing – review & editing. **Giuseppe Milano:** Writing – review & editing, Conceptualization.

Declaration of competing interest

The authors declare the following financial interests/personal relationships which may be considered as potential competing interests: Giuseppe Milano reports financial support was provided by University of Naples Federico II. Giuseppe Milano reports a relationship with University of Naples Federico II that includes: employment. If there are other authors, they declare that they have no known competing financial interests or personal relationships that could have appeared to influence the work reported in this paper.

Acknowledgments

Giuseppe Milano and Giuseppe Scherillo acknowledge University of Naples Federico II for funding grant POLYMANTRA.

Data availability

No data was used for the research described in the article.

References

[1] A. Bhattacharya, B.N. Misra, Grafting: a versatile means to modify polymers techniques, factors and applications, Prog. Polym. Sci. 29 (2004) 767–814.
[2] T.A. Sherazi, Graft polymerization, in: Encyclopedia of Membranes, Springer, 2016, pp. 886–887.
[3] P. Purohit, A. Bhatt, R.K. Mittal, M.H. Abdellattif, T.A. Farghaly, Polymer grafting and its chemical reactions, Front. Bioeng. Biotechnol. 10 (2023).
[4] R. Yin, J. Tarnsangpradit, A. Gul, J. Jeong, X. Hu, Organic nanoparticles with tunable size and rigidity by hyperbranching and cross-linking using microemulsion atrp, Proc. Natl. Acad. Sci. (2024).
[5] S. Hansson, V. Trouillet, T. Tischer, A.S. Goldmann, A. Carlmark, C. Barner-Kowollik, E. Malmström, Grafting efficiency of synthetic polymers onto biomaterials: A comparative study of grafting-from versus grafting-to, Biomacromolecules 14 (2013) 64–74.
[6] I.N. Haugan, M.J. Maher, A.B. Chang, T.-P. Lin, R.H. Grubbs, M.A. Hillmyer, F.S. Bates, Consequences of grafting density on the linear viscoelastic behavior of graft polymers, ACS Macro Lett. 7 (2018) 525–530.
[7] S.K. Kumar, N. Jouault, B. Benicewicz, T. Neely, Nanocomposites with polymer grafted nanoparticles, Macromolecules 46 (2013) 3199.
[8] A.J. Chancellor, B.T. Seymour, B. Zhao, Characterizing polymer-grafted nanoparticles: From basic defining parameters to behavior in solvents and self-assembled structures, Anal. Chem. 91 (2019) 6391–6402.
[9] M.J.A. Hore, L.T.J. Korely, S.K. Kumar, Polymer-grafted nanoparticles, J. Appl. Phys. 128 (2020) 030401.
[10] C. Feng, X. Huang, Polymer brushes: Efficient synthesis and applications, Acc. Chem. Res. 51 (2018) 2314–2323.
[11] S. Wang, Z. Wang, J. Li, L. Li, W. Hu, Surface-grafting polymers: from chemistry to organic electronics, Mater. Chem. Front. 4 (2019) 692–714.
[12] Y. Liu, J. Wang, F. Cui, Y. Han, J. Yan, X. Qin, Surface-initiated atom transfer radical polymerization for the preparation and applications of brush-modified inorganic nanoparticles, Adv. Mater. (2024).
[13] J.H. Koo, Polymer Nanocomposites: Processing, Characterization, and Application, McGraw-Hill, 2016.
[14] A.C. Balazs, T. Emrick, T.P. Russell, Nanoparticle polymer composites: where two small worlds meet, Science 314 (2006) 1107.
[15] D. Brown, V. Marcadon, P. Mèlè, N.D. Albèrola, Effect of filler particle size on the properties of model nanocomposites, Macromolecules 41 (2008) 1499.
[16] P. Akcora, H. Liu, S.K. Kumar, J. Moll, Y. Li, B.C. Benicewicz, L.S. Schadler, D. Acechin, A.Z. Panagiotopoulos, V. Pyramitsyn, V. Ganesan, J. Ilavsky, P. Thiyagarajan, R.H. Colby, J.F. Douglas, Anisotropic self-assembly of spherical polymer-grafted nanoparticles, Nat. Mater. 8 (2009) 354.
[17] S.K. Kumar, V. Ganesan, R.A. Riggleman, Perspective: Outstanding theoretical questions in polymer-nanoparticle hybrids, J. Chem. Phys. 147 (2017) 020901.
[18] G.G. Vogiatzis, D. Theodorou, Multiscale molecular simulations of polymer–matrix nanocomposites or what molecular simulations have taught us about the fascinating nanoworld, Arch. Comput. Methods Eng. 25 (2018) 591–645.
[19] Q. Lan, L.F. Francis, F.S. Bates, Silica nanoparticle dispersions in homopolymer versus block copolymer, J. Polym. Sci. Polym. Phys. 45 (2007) 2284.
[20] P. Akcora, S.K. Kumar, J. Moll, S. Lewis, L.S. Schadler, Y. Li, B.C. Benicewicz, A. Sandy, S. Narayanan, J. Ilavsky, P. Thiyagarajan, R.H. Colby, J.F. Douglas, "gel-like" mechanical reinforcement in polymer nanocomposite melts, Macromolecules 43 (2010) 1003.
[21] D. Sunday, J. Ilavsky, D.L. Green, A phase diagram for polymer-grafted nanoparticles in homopolymer matrices, Macromolecules 45 (2012) 4007.
[22] T.V.M. Ndoro, E. Voyiatzis, A. Ghanbari, D.N. Theodorou, M.C. Böhm, F. Müller-Plathe, Interface of grafted and ungrafted silica nanoparticles with a polystyrene matrix: Atomistic molecular dynamics simulations, Macromolecules 44 (2011) 2316.
[23] T.V.M. Ndoro, M.C. Böhm, F. Müller-Plathe, Interface and interphase dynamics of polystyrene chains near grafted and ungrafted silica nanoparticles, Macromolecules 45 (2012) 171.
[24] M. Rahimi, I. Iriarte-Carretero, A. Ghanbari, M.C. Böhm, F. Müller-Plathe, Mechanical behavior and interphase structure in a silica-polystyrene nanocomposite under uniaxial deformation, Nanotechnology 23 (2012) 305702.
[25] A. Ghanbari, T.V.M. Ndoro, F. Leroy, M. Rahimi, M.C. Böhm, F. Müller-Plathe, Interphase structure in silica-polystyrene nanocomposites: A coarse-grained molecular dynamics study, Macromolecules 45 (2012) 572.
[26] A. Ghanbari, M. Rahimi, J. Dehghany, Influence of surface grafted polymers on the polymer dynamics in a silica-polystyrene nanocomposite: A coarse-grained molecular dynamics investigation, J. Phys. Chem. C 117 (2013) 25069.
[27] E. Voyiatzis, F. Müller-Plathe, M.C. Böhm, Influence of nanoparticle inclusion on the cavity size distribution and accessible volume in polystyrene-silica nanocomposites, Polymer 101 (2016) 107.
[28] S. Pfaller, G. Possart, P. Steinmann, M. Rahimi, F. Müller-Plathe, M.C. Böhm, Investigation of interphase effects in silica-polystyrene nanocomposites based on a hybrid molecular-dynamics-finite-element simulation framework, Phys. Rev. E 93 (2016) 052505.
[29] L.M. Hall, A. Jayaraman, K.S. Schweizer, Molecular theories of polymer nanocomposites, Curr. Opin. Solid State Mater. Sci. 14 (2010) 38.
[30] T.B. Martin, A. Jayaraman, Identifying the ideal characteristics of the grafted polymer chain length distribution for maximizing dispersion of polymer grafted nanoparticles in a polymer matrix, Macromolecules 46 (2013) 9144.
[31] T.B. Martin, A. Jayaraman, Polydisperse homopolymer grafts stabilize dispersions of nanoparticles in a chemically identical homopolymer matrix: an integrated theory and simulation study, Soft. Matter. 9 (2013) 6876.
[32] T.B. Martin, A. Jayaraman, Effect of matrix bidispersity on the morphology of polymer-grafted nanoparticle-filled polymer nanocomposites, J. Polym. Sci. B 52 (2014) 1661.
[33] F. Lo Verso, L. Yelash, S.A. Egorov, K. Binder, Interactions between polymer brush-coated spherical nanoparticles: The good solvent case, J. Chem. Phys. 135 (2011) 214902.
[34] P.M. Dodd, A. Jayaraman, Monte carlo simulations of polydisperse polymers grafted on spherical surfaces, J. Polym. Sci. B 50 (2012) 694.
[35] F. Lo Verso, L. Yelash, K. Binder, Dynamics of macromolecules grafted in spherical brushes under good solvent conditions, Macromolecules 46 (2011) 4716–4722.
[36] C.J. Revelas, A.P. Sgouros, A.T. Lakkas, D. Theodorou, Tailoring nanoparticle orientation in polymer matrices via nonuniform grafting: Implications for nanoparticle dispersions and self-assembled nanocomposite morphologies, ACS Appl. Nano Mater. 7 (2024) 19329–19340.
[37] C. Chevigny, J. Jestin, D. Gigmes, R. Schweins, E. Di Cola, F. Dalmas, D. Bertin, F. Bouè, Wet-to-dry conformational transition of polymer layers grafted to nanoparticles in nanocomposite, Macromolecules 43 (2010) 4833.
[38] C. Chevigny, F. Dalmas, E. Di Cola, D. Gigmes, D. Bertin, F. Boue, J. Jestin, Polymer-grafted-nanoparticles nanocomposites: Dispersion, grafted chain conformation, and rheological behavior, Macromolecules 44 (2011) 122.
[39] A.P. Sgouros, C.J. Revelas, A.T. Lakkas, D. Theodorou, Potential of mean force between bare or grafted silica/polystyrene surfaces from self-consistent field theory, Polymers 13 (2021) 1197.
[40] A.T. Lakkas, A.P. Sgouros, C.J. Revelas, D. Theodorou, Structure and thermodynamics of grafted silica/polystyrene dilute nanocomposites investigated through self-consistent field theory, Soft Matter 17 (2021) 4077–4097.
[41] A.P. Sgouros, C.J. Revelas, A.T. Lakkas, D. Theodorou, Solvation free energy of dilute grafted (nano)particles in polymer melts via the self-consistent field theory, J. Phys. Chem. B 126 (2022) 7454–7474.

[42] C.J. Revelas, A.P. Sgouros, A.T. Lakkas, D. Theodorou, Addressing nanocomposite systems via 3d-scft: Assessment of smearing approximation and irregular grafting distributions, Macromolecules 56 (2023) 1731–1746.
[43] C.M. Bates, M.J. Maher, D.W. Janes, C.J. Ellison, C.G. Willson, Block copolymer lithography, Macromolecules 47 (2014) 2–12.
[44] P. Müller-Buschbaum, Gisaxs and gisans as metrology technique for understanding the 3d morphology of block copolymer thin films, Eur. Polym. J. 81 (2016) 470–493.
[45] P. Mansky, Y. Liu, E. Huang, T.P. Russell, C. Hawker, Controlling polymer-surface interactions with random copolymer brushes, Science 275 (1997) 1458–1460.
[46] B. Zdyrko, I. Luzinov, Polymer brushes by the "grafting to" method, Macromol. Rapid Commun. 32 (2011) 859–869.
[47] R. Chiarcos, M. Perego, M. Laus, Polymer brushes by grafting to reaction in melt: New insights into the mechanism, Macromol. Chem. Phys. 224 (2023) 2200400.
[48] V. Ganesan, A. Jayaraman, Theory and simulation studies of effective interactions, Phase Behav. Morphol. Polym. Nanocomposites, Soft Matter 10 (2014) 13.
[49] Y. Tang, Y. Liu, D. Zhang, J. Zheng, Perspectives on theoretical models and molecular simulations of polymer brushes, Langmuir 40 (2024) 1487–1502.
[50] R. Ishraaq, S. Das, All-atom molecular dynamics simulations of polymer and polyelectrolyte brushes, Chem. Commun. 60 (2024) 6093.
[51] E. Mohammadi, S.Y. Joshi, S.A. Deshmukh, A review of computational studies of bottlebrush polymers, Comput. Mater. Sci. 199 (2021) 110720.
[52] K. Schweizer, J. Curro, Ntegral-equation theory of the structure of polymer melts, Phys. Rev. Lett. 58 (1987) 246–249.
[53] T.B. Martin, I.T.E. Gartner, R.L. Jones, C.R. Snyder, A. Jayaraman, pyprism: A computational tool for liquid-state theory calculations of macromolecular materials, Macromolecules 51 (2018) 2906–2922.
[54] C.E. Woodward, A.A. Yethiraj, Density-functional theory for inhomogeneous polymer-solutions, J. Chem. Phys. 100 (1994) 3181–3186.
[55] K.F. Freed, Interrelation between density functional and self-consistent-field formulations for inhomogeneous polymer systems, J. Chem. Phys. 103 (1995) 3230.
[56] K. Binder, A. Milchev, Polymer brushes on flat and curved surfaces: How computer simulations can help to test theories and to interpret experiments, J. Polym. Sci. Part B: Polym. Phys. 50 (2012) 1515–1555.
[57] X. Song, J. Man, Y. Qiu, J. Wang, J. Liu, R. Li, Y. Zhang, J. Li, J. Li, Y. Chen, Design, preparation, and characterization of lubricating polymer brushes for biomedical applications, Acta Biomater. 175 (2024) 76–105.
[58] T. Kawakatsu, Statistical Physics of Polymers, Springer, Berlin, 2004.
[59] G. Milano, G.J.A. Sevink, Z.-Y. Lu, Y. Zhao, A. De Nicola, G. Munaò, T. Kawakatsu, Hybrid particle-field molecular dynamics: A primer, in: Comprehensive Computational Chemistry, Elsevier, 2024, pp. 636–659.
[60] A. De Nicola, T. Kawakatsu, G. Milano, Generation of well relaxed all atom models of large molecular weight polymer melts: A hybrid particle-continuum approach based on particle-field molecular dynamics simulations, J. Chem. Theory Comput. 10 (2014) 5651.
[61] Y. Zhao, M. Byshkin, Y. Cong, T. Kawakatsu, L. Guadagno, A. De Nicola, N.S. Yu, G. Milano, B. Dong, Self-assembly of carbon nanotubes in polymer melts: Simulation of structural and electrical behaviour by hybrid particle-field molecular dynamics, Nanoscale 8 (2016) 15538.
[62] G. Donati, A. De Nicola, G. Munaò, M. Byshkin, L. Vertuccio, L. Guadagno, R. Le Goff, G. Milano, Simulation of self-heating process on the nanoscale: a multiscale approach for molecular models of nanocomposite materials, Nanoscale Adv. 2 (2020) 3164–3180.
[63] A. De Nicola, T. Kawakatsu, F. Müller-Plathe, G. Milano, Fast relaxation of coarse-grained models of polymer interphases by hybrid particle-field molecular dynamics: Polystyrene-silica nanocomposites as an example, Eur. Phys. J. Spec. Top. 225 (2016) 1817.
[64] S. Caputo, V. Hristov, A. De Nicola, H. Herbst, A. Pizzirusso, G. Donati, G. Munaò, A.R. Albunia, G. Milano, Efficient hybrid particle-field coarse-grained model of polymer filler interactions: Multiscale hierarchical structure of carbon black particles in contact with polyethylene, J. Chem. Theory Comput. (2021).
[65] C. Brondi, A. Baldanza, R. Chiarcos, M. Laus, G. Scherillo, G. Mensitieri, G. Milano, Partition by molecular weight of polymer brushes: A combined reactive grand canonical monte carlo and self-consistent field investigation of grafting to processes, Polymer 294 (2024) 126737.
[66] G. Milano, T. Kawakatsu, Hybrid particle-field molecular dynamics simulations for dense polymer systems, J. Chem. Phys. 130 (2009) 214106.
[67] E. Helfand, Theory of inhomogeneous polymers: Fundamentals of the gaussian random-walk model, J. Chem. Phys. 62 (1975) 999–1005.
[68] Y. Zhao, A. De Nicola, T. Kawakatsu, G. Milano, Hybrid particle-field molecular dynamics simulations: Parallelization and benchmarks, J. Comput. Chem. 33 (2012) 868.
[69] D. Frenkel, B. Smit, Understanding Molecular Simulations: From Algorithms to Applications, second ed., Academic Press, New York, 2002.
[70] J.M.H.M. Scheutjens, G.J. Fleer, Statistical theory of the adsorption of interacting chain molecules. 1. partition function, segment density distribution, and adsorption isotherms, J. Phys. Chem. 83 (1979) 1619–1635.
[71] H.-J. Qian, P. Carbone, X. Chen, H.A. Karimi-Varzaneh, C.C. Liew, F. Müller-Plathe, Temperature-transferable coarse-grained potentials for ethylbenzene, polystyrene, and their mixtures, Macromolecules 41 (2008) 9919.
[72] G. Munaò, A. Pizzirusso, A. Kalogirou, A. De Nicola, T. Kawakatsu, F. Müller-Plathe, G. Milano, Molecular structure and multi-body interactions in silica-polystyrene nanocomposites, Nanoscale 10 (2018) 21656.
[73] G. Munaò, A. De Nicola, F. Müller-Plathe, T. Kawakatsu, A. Kalogirou, G. Milano, Influence of polymer bidispersity on the effective particle–particle interactions in polymer nanocomposites, Macromolecules 52 (2019) 8826–8839.
[74] I. Borukhov, L. Leibler, Enthalpic stabilization of brush-coated particles in a polymer melt, Macromolecules 35 (2002) 5171–5182.
[75] G.D. Smith, D. Bedrov, Dispersing nanoparticles in a polymer matrix: Are long, dense polymer tethers really necessary? Langmuir 25 (2009) 11239.
[76] F. Lo Verso, S.A. Egorov, K. Binder, Interaction between polymer brush-coated spherical nanoparticles: Effect of solvent quality, Macromolecules 45 (2012) 8802–8902.
[77] D. Meng, S.K. Kumar, J.M.D. Lane, G.S. Grest, Effective interactions between grafted nanoparticles in a polymer matrix, Soft Matter 8 (2012) 5002.
[78] H.C. Hamaker, The london-van der waals attraction between spherical particles, Physica 4 (1937) 1058.
[79] G. Munaò, A. Correa, A. Pizzirusso, G. Milano, On the calculation of the potential of mean force between atomistic nanoparticles, EPJ E 41 (2018) 38.
[80] G. Munaò, P. O'Toole, T.S. Hudson, D. Costa, C. Caccamo, F. Sciortino, A. Giacometti, Cluster formation and phase separation in heteronuclear janus dumbbells, J. Phys.: Condens. Matter. 27 (2015) 234101.
[81] A.J. Archer, D. Pini, R. Evans, L. Reatto, Model colloidal fluid with competing interactions: Bulk and interfacial properties, J. Chem. Phys. 126 (2007) 014104.
[82] A.J. Archer, C. Ionescu, D. Pini, L. Reatto, Theory for the phase behaviour of a colloidal fluid with competing interactions, J. Phys.: Condens. Matter. 20 (2008) 415106.
[83] A.L. Frischknecht, A. Yethiraj, Two- and three-body interactions among nanoparticles in a polymer melt, J. Chem. Phys. 134 (2011) 174901.
[84] S.J. Park, S. Kim, D. Yong, Y. Choe, J. Bang, J.U. Kim, Interactions between brush-grafted nanoparticles within chemically identical homopolymers: the effect of brush polydispersity, Soft Matter 14 (2018) 1026.
[85] A. Rungta, B. Natarajan, T. Neely, D. Dukes, L.S. Schadler, B.C. Benicewicz, Grafting bimodal polymer brushes on nanoparticles using controlled radical polymerization, Macromolecules 45 (2012) 9303.
[86] B. Natarajan, T. Neely, A. Rungta, B.C. Benicewicz, L.S. Schadler, Thermomechanical properties of bimodal brush modified nanoparticle composites, Macromolecules 46 (2013) 4909.
[87] Y. Li, P. Tao, A. Viswanath, B.C. Benicewicz, L.S. Schadler, Bimodal surface ligand engineering: The key to tunable nanocomposites, Langmuir 29 (2013) 1211.
[88] C. Triebel, P. Kunzelmann, M. Blankeburg, H. Münstedt, Elasticity of polystyrene melts filled with silica nanoparticles: Influence of matrix polydispersity, Polymer 52 (2011) 3621.
[89] T.B. Martin, P.M. Dodd, A. Jayaraman, Polydispersity for tuning the potential of mean force between polymer grafted nanoparticles in a polymer matrix, Phys. Rev. Lett. 110 (2013) 018301.
[90] R. Shi, H.-J. Qian, Z.-Y. Lu, Computer simulation study on the self-assembly of unimodal and bimodal polymer-grafted nanoparticles in a polymer melt, Phys. Chem. Chem. Phys. 19 (2017) 16524.
[91] F. Sciortino, S. Mossa, E. Zaccarelli, P. Tartaglia, Equilibrium cluster phases and low-density arrested disordered states: The role of short-range attraction and long-range repulsion, Phys. Rev. Lett. 93 (2004) 055701.
[92] Z. Preisler, T. Vissers, G. Munaò, F. Smallenburg, F. Sciortino, Equilibrium phases of one-patch colloids with short-range attractions, Soft Matter 10 (2014) 5121.
[93] K. Sparnacci, R. Chiarcos, V. Gianotti, M. Laus, T.J. Giammaria, M. Perego, G. Munaò, G. Milano, A. De Nicola, M. Haese, L.P. Kreuzer, T. Widmann, P. Müller-Buschbaum, Effect of trapped solvent on the interface between ps-b-pmma thin films and p(s-r-mma) brush layers, ACS Appl. Mater. Interfaces 12 (2020) 7777–7787.
[94] H. Morita, T. Kawakatsu, Dynamic density functional study on the structure of thin polymer blend films with a free surface, Macromolecules 34 (2001) 8777–8783.
[95] A. Galuschko, L. Spirin, T. Kreer, A. Johner, C. Pastorino, J. Wittmer, J. Baschnagel, Frictional forces between strongly compressed, nonentangled polymer brushes: Molecular dynamics simulations and scaling theory, Langmuir 26 (2010) 6418–6429.

[96] M. Laus, R. Chiarcos, V. Gianotti, D. Antonioli, K. Sparnacci, G. Munaò, G. Milano, A. De Nicola, M. Perego, Evidence of mechanochemical control in grafting to reactions of hydroxy-terminated statistical copolymers, Macromolecules 54 (2021) 499–508.
[97] D. Antonioli, R. Chiarcos, V. Gianotti, M. Terragno, M. Laus, G. Munaò, G. Milano, A. De Nicola, M. Perego, Inside the brush: partition by molecular weight in grafting to reactions from melt, Polym. Chem. 12 (2021) 6358.
[98] R. Chiarcos, D. Antonioli, V. Gianotti, M. Laus, G. Munaò, G. Milano, A. De Nicola, M. Perego, Short vs. long chains competition during grafting to process from melt, Polym. Chem. 13 (2022) 3904.
[99] N. Metropolis, A.W. Rosenbluth, A.H. Teller, Equation of state calculations by fast computing machines, J. Chem. Phys. 21 (1953) 1087–1092.
[100] C.C. van der Linden, F.A. Leermakers, G.J. Fleer, Adsorption of semiflexible polymer, Macromolecules 29 (1996) 1172–1178.